Transverse collective flow and midrapidity emission of isotopically identified light charged particles

Z. Kohley,[1,2,*] L. W. May,[1,2] S. Wuenschel,[1,2] M. Colonna,[3] M. Di Toro,[3,4] M. Zielinska-Pfabe,[5] K. Hagel,[2] R. Tripathi,[2] A. Bonasera,[2,3] G. A. Souliotis,[2,6] D. V. Shetty,[2,†] S. Galanopoulos,[2] M. Mehlman,[2,7] W. B. Smith,[2] S. N. Soisson,[1,2] B. C. Stein,[1,2] and S. J. Yennello[1,2]

[1]*Chemistry Department, Texas A&M University, College Station, Texas 77843, USA*
[2]*Cyclotron Institute, Texas A&M University, College Station, Texas 77843, USA*
[3]*Laboratori Nazionali del Sud, INFN, I-95123 Catania, Italy*
[4]*Physics and Astronomy Department, University of Catania, Italy*
[5]*Smith College, Northampton, Massachusetts, USA*
[6]*Laboratory of Physical Chemistry, Department of Chemistry, National and Kapodistrian University of Athens, Athens GR-15771, Greece*
[7]*Physics and Astronomy Department, Texas A&M University, College Station, Texas 77843, USA*

(Received 13 June 2010; revised manuscript received 17 January 2011; published 1 April 2011)

The transverse flow and relative midrapidity yield of isotopically identified light charged particles (LCPs) has been examined for the 35 MeV/nucleon ^{70}Zn + ^{70}Zn, ^{64}Zn + ^{64}Zn, and ^{64}Ni + ^{64}Ni systems. A large enhancement of the midrapidity yield of the LCPs was observed relative to the yield near the projectile rapidity. In particular, this enhancement was increased for the more neutron-rich LCPs demonstrating a preference for the production of neutron-rich fragments in the midrapidity region. Additionally, the transverse flow of the LCPs was extracted, which provides insight into the average movement of the particles in the midrapidity region. Isotopic and isobaric effects were observed in the transverse flow of the fragments. In both cases, the transverse flow was shown to decrease with an increasing neutron content in the fragments. A clear inverse relationship between the transverse flow and the relative midrapidity yield is shown. The increased relative midrapidity emission produces a decreased transverse flow. The stochastic mean-field model was used for comparison to the experimental data. The results showed that the model was able to reproduce the general isotopic and isobaric trends for the midrapidity emission and transverse flow. The sensitivity of these observables to the density dependence of the symmetry energy was explored. The results indicate that the transverse flow and midrapidity emission of the LCPs are sensitive to the denisty dependence of the symmetry energy.

DOI: 10.1103/PhysRevC.83.044601 PACS number(s): 25.70.Pq, 21.65.Ef

I. INTRODUCTION

Improving our understanding of the nuclear equation of state (EoS) is an important goal for the field of nuclear science. Currently, the EoS for symmetric nuclear matter is thought to be relatively constrained, while predictions for the EoS of asymmetric nuclear matter can still vary widely [1–3]. Recent experimental results are being used to apply constraints to the asymmetric part of the EoS, or density dependence of the symmetry energy [$E_{\rm sym}(\rho)$] [3–6]. Constraining the density dependence of the symmetry energy is essential for understanding the fundamental nucleon-nucleon interaction and has important astrophysical implications [3,5,7–13].

Heavy-ion collisions (HICs) provide a unique opportunity to examine the nuclear EoS because nuclear matter is produced at temperatures, densities, and neutron-to-proton (N/Z) ratios away from that of ground-state nuclei. In the examination of peripheral and semiperipheral intermediate-energy HICs an important source of particle production has been found to originate from a midrapidity, or neck, region between the quasiprojectile (QP) and quasitarget (QT) [14–19]. Experimental results have demonstrated an increased neutron-to-proton ratio in this midrapidity region in comparison to the quasiprojectile source through the examination of isotopically resolved fragments, as well as the detection of free neutrons [18–26]. For example, Lukasik *et al.* showed that 65%–70% of the total ^{3}H production can be attributed to the midrapidity region [18]. Furthermore, it has been suggested that the necklike structure represents a low-density region of nuclear matter between the higher density QP and QT [27,28]. Thus, the neck region can provide an opportunity to examine dilute neutron-rich nuclear matter. The study of this low-density asymmetric nuclear matter should provide sensitivity to the nuclear EoS. Theoretical models have shown that the isospin content and production of intermediate mass fragments (IMFs) in the neck region could be used to probe the nuclear EoS [17,29–31].

The transverse flow is closely connected to the midrapidity emission properties and describes the average movement of the particles in the midrapidity region. While transverse flow measurements have been very important in helping elucidate the EoS for symmetric nuclear matter [32,33], they have been consistently discussed as a probe to examine the density dependence of the symmetry energy [3,34–37]. Pak *et al.* demonstrated that both the transverse collective flow for $Z = 1$–3 particles and the balance energy increased with an increasing neutron-to-proton ratio of the system, $(N/Z)_{\rm sys}$

*zkohley@comp.tamu.edu; current address: Physics Division, Oak Ridge National Laboratory, Oak Ridge, TN 37831, USA
†Current address: Physics Department, Western Michigan University, Kalamazoo, MI 49008, USA

 ©2011 American Physical Society

[38,39]. This was the first evidence that the collective flow was sensitive to the isospin concentration of the colliding system. The isospin dependence of the transverse flow and balance energy were attributed to the isospin-dependent potential and in-medium nucleon-nucleon cross sections through comparisons with a Boltzmann-Uehling-Uhlenback (BUU) and quantum molecular dynamics (QMD) model [40,41]. Scalone *et al.* used a Boltzmann-Nordheim-Vlasov (BNV) simulation to demonstrate that the isospin dependence observed by Pak *et al.* was sensitive to the density dependence of the symmetry energy [42].

Differences between the free neutron and free proton transverse collective flows have been predicted to be strongly sensitive to $E_{\rm sym}(\rho)$ [43–45]. However, obtaining accurate energy and angular measurements of free neutrons, along with charged particles, is a difficult task. Currently, experimental data from the FOPI/LAND detectors are being used to extract neutron and proton collective flows to examine the sensitivity to the density dependence of the symmetry energy [46,47]. The results will be used to plan a dedicated experiment in an attempt to apply high-density constraints to the symmetry energy.

Scalone *et al.* showed that a comparison of the flow parameter from ^{3}H and ^{3}He light clusters would exhibit a similar dependence on $E_{\rm sym}(\rho)$ as the neutron and proton flows [42]. The simulations showed that for a stiff-symmetry energy parametrization the ^{3}He clusters should have an estimated 20% larger flow than the ^{3}H clusters in midperipheral collisions from a 55 MeV/nucleon ^{58}Fe + ^{58}Fe reaction system [42]. In the case of a soft parametrization, the difference in the flow parameter between the ^{3}H and ^{3}He clusters disappeared [35,42]. Thus, by measuring the flow parameter of the ^{3}H and ^{3}He clusters one should be able to gain insight into the density dependence of the symmetry energy. Recently, Yong *et al.*, using a BUU calculation, have demonstrated that the ^{3}H and ^{3}He flow, from a 400 MeV/nucleon reaction, could be used to probe the density dependence of the symmetry energy at suprasaturation densities [48].

In the this paper, the relative midrapidity emission and the transverse flow of isotopically identified light charged particles has been investigated for the 35 MeV/nucleon ^{70}Zn + ^{70}Zn, ^{64}Zn + ^{64}Zn, and ^{64}Ni + ^{64}Ni systems. The experimental details are provided in Sec. II, along with a brief description of the stochastic mean-field (SMF) model [49,50]. The experimental and simulated midrapidity yields and transverse flow results are presented in Sec. III. Last, the conclusions and acknowledgments are provided in Secs. IV and II A, respectively.

II. EXPERIMENTAL AND THEORETICAL DETAILS

A. Detector setup

The K500 Superconducting Cyclotron at the Texas A&M University Cyclotron Institute was used to produce beams of ^{70}Zn, ^{64}Zn, and ^{64}Ni at 35 MeV/nucleon which were collided with ^{70}Zn (95%), ^{64}Zn (99.8%), and ^{64}Ni (98.0%) self-supporting targets, respectively. The reaction products were measured using the 4π NIMROD-ISiS array (Neutron Ion Multi-detector for Reaction Oriented Dynamics with the Indiana Silicon Sphere) [51]. The entire charged-particle array is housed inside the Texas A&M Neutron Ball [52], which provides an average neutron multiplicity.

The charged-particle array consists of 14 concentric rings, labeled rings 2–15, covering from 3.6° to 167.0° in laboratory. Rings 2–9, ranging from 3.6° to 45.0°, have the same geometry as the INDRA detector [53] and rings 10–15 are of the ISiS geometry [54]. Rings 2–9 each consist of 10 single telescope modules and 2 supertelescope modules. A single telescope module contains a 150- or 300-μm silicon detector placed in front of a thallium-doped cesium iodide crystal, CsI(Tl). The supertelescopes have both a 150-μm and a 500-μm Si placed in front of the CsI(Tl) crystal. Rings 10 and 11 each have 18 single telescope modules with 300-μm Si-CsI(Tl) detectors. Rings 12–15 each contain 18 single telescope detectors, with 500-μm-thick silicon.

Three methods of particle identification are available in the NIMROD-ISiS array. In rings 2–11 pulse shape analysis of the CsI(Tl)-PMT (thallium-doped cesium iodide with a photomultiplier tube) signals provided clear separation of neutron/γ, ^{1}H, ^{2}H, ^{3}H, ^{3}He, ^{4}He, and ^{6}He particles. Isotopic resolution of heavier mass fragments was achieved through $\Delta E - E$ measurements from the Si-CsI (single telescope) and Si-Si (supertelescope) modules. In the forward angle rings, isotopic resolution of $1 \leqslant Z \leqslant 17$ particles and elemental resolution up to the charge of the beam was obtained through the Si-CsI and Si-Si detector modules. Detector thresholds limited the isotopic resolution to $1 \leqslant Z \leqslant 2$ particles for the backward angles. A linearization procedure was utilized to complete the particle identification [51,55].

The relationship derived by Tasson-Got [56] was used to relate the light output from the CsI to the particle energy. Proton (30 and 55 MeV), ^{2}H (60 MeV), and ^{4}He (100 MeV) calibration beams were used to help constrain the parameters of the CsI calibration. The punch-through energies of the identified fragments, along with a ^{228}Th source and a 500-MeV ^{20}Ne calibration beam, were used to constrain the silicon detector calibrations. The resulting energy spectra were compared to previous NIMROD data sets for 35 MeV/nucleon systems of similar size and showed excellent agreement [57,58].

B. Event selection and reaction plane determination

In examining the midrapidity emission and transverse collective flow it is important to estimate the centrality of the collisions because the strongest signatures are observed in midperipheral collisions [18,35,38,59]. The impact parameter for the experimental data was estimated using minimum bias distributions of the neutron multiplicity plotted against the charged-particle multiplicity for each system. Three bins were created from the two-dimensional (2D) distributions such that each bin would represent a $b/b_{\rm max}$, or $b_{\rm red}$, width of 0.33 if one assumes a corresponding triangular impact parameter distribution. A simulation with the constrained molecular dynamics model [60], filtered for experimental acceptance, confirmed this method of impact parameter selection. Thus,

the bin representing the events with the highest neutron and charged-particle multiplicities should represent the most central collisions, while the low-multiplicity events should represent the most peripheral collisions. In the following, the transverse flow is examined for the midperipheral collisions, which should represent $b_{\rm red} \cong 0.33$–0.66. To ensure that a well-characterized system was considered an event criterion was imposed such that the total detected charge for an event must be greater than 40% of the total charge in the colliding system.

The azimuthal correlation method [61] was used for the reaction plane reconstruction from the transverse momentum of the fragments of each event. The azimuthal correlation method does not differentiate between the forward, quasiprojectile, and the backward, quasitarget, sides of the flow. Therefore, the forward flow side of the reaction plane was determined using the transverse momentum analysis method [62]. The particle of interest (POI) was removed from the calculation of the reaction plane to avoid autocorrelations [61–63]. Thus, the reaction plane was calculated for each particle in an event rather than on an event-by-event basis. A velocity boost was applied to each particle used in the calculation of the reaction plane to account for momentum conservation [61,64].

The method described in Ref. [61] was used to estimate the accuracy of the reaction plane resolution. Each event was randomly divided into two subevents and the reaction plane was calculated for each of the subevents. The difference in the reaction-plane angle between the subevents, $\Delta\phi_{12}$, was then calculated. The width of the $\Delta\phi_{12}$ distribution can be related to the standard deviation between the reconstructed and true reaction plane, which is a representation of the reaction-plane resolution [61]. The standard deviation between the true and reconstructed reaction plane was estimated to be $\sim 27^{\circ}$, which demonstrates an improved accuracy in comparison to previous experiments [61].

C. Stochastic mean-field model

The midrapidity emission and transverse flow of the light charged particles (LCPs) was investigated within the framework of the SMF model [49,50]. The SMF model uses the test-particle method to solve the Boltzmann-Langevin transport equation [65]. A momentum-dependent potential was used in the simulation and the density dependence of the symmetry energy was varied [49,50]. In the following, the stiff-SMF and soft-SMF results will refer to the results of the SMF model where the potential produces a stiff and soft, respectively, density dependence of the symmetry energy. The simulation was stopped at 120 fm/c and a phase-space coalescence was applied to identify the fragments [66]. Thus, theoretical simulation provides information about the initial fragment distribution.

III. RESULTS AND DISCUSSION

In the following section, both the LCP yield and $\langle P_x/A \rangle$ are examined as a function of the reduced rapidity, which is defined as

$$Y_r = \frac{Y_{\rm c.m.}}{Y_{\rm c.m.,proj}}, \tag{1}$$

where $Y_{\rm c.m.}$ is the center-of-mass rapidity of the LCP and $Y_{\rm c.m.,proj}$ is the center-of-mass rapidity of the projectile [67]. In mass symmetric systems, this conveniently scales the rapidity such that $Y_r = 1\,(-1)$ is equal to the projectile (target) rapidity. Therefore, the midrapidity region is easily defined around $Y_r = 0$.

A. Midrapidity emission

In Fig. 1 the yields of the different isotopically identified LCPs (solid black circles) are shown as a function of the reduced rapidity from the experimental data (the SMF results are discussed below). The observed asymmetry in the distributions are attributable to the decreased efficiency for detection of the LCPs at the backward laboratory angles owing to the lower laboratory-frame energy of the fragments. Therefore, we focus on the forward rapidity region ($Y_r > 0$), where the detector capabilities are much better. The results demonstrate a clear preference for emission around the midrapidity region ($Y_r = 0$) for all LCPs, in comparison to where one would expect to observe the decay of the QP, near $Y_r = 1$.

To further explore the enhanced midrapidity emission the relative yield of the LCPs was calculated as

$$R_{\rm yield}^{\rm mid} = \frac{{\rm Yield}^{\rm midrapidity}}{{\rm Yield}^{\rm QP}/2}, \tag{2}$$

where the midrapidity yield (Yield$^{\rm midrapidity}$) is defined as the yield from $0.0 \leqslant Y_r \leqslant 0.5$ and the QP yield (Yield$^{\rm QP}$) is defined as the yield from $0.5 \leqslant Y_r \leqslant 1.5$. Notice that Yield$^{\rm QP}$ was scaled by a factor of 2 in Eq. (2) because a larger range was used in defining the QP yield. It is important to recognize that these definitions for the midrapidity and QP yield are very simple estimations; however, they should provide some insight into the relative production of the LCPs.

The $R_{\rm yield}^{\rm mid}$ values for the LCPs are presented in Fig. 2 as a function of the charge times mass (ZA) for the three reaction systems. A distinct trend is observed demonstrating an increased midrapidity yield for the more neutron-rich LCPs. For the $Z = 1$ isotopes, the largest value of $R_{\rm yield}^{\rm mid}$ is shown for ^{3}H ($N/Z = 2.0$) followed by the ^{2}H ($N/Z = 1.0$) and, last, ^{1}H ($N/Z = 0.0$). The same trend is also present for the $Z = 2$ isotopes with the ^{6}He ($N/Z = 2.0$) showing the largest midrapidity enhancement and the ^{3}He ($N/Z = 0.5$) showing the least. Additionally, an isobaric comparison between ^{3}H and ^{3}He, shows the same trend with a larger fraction of ^{3}H being produced in the midrapidity region than ^{3}He fragments. While the actual N/Z of the midrapidity region relative to the QP region cannot be determined without free neutron detection [20], these results demonstrate a strong preference for the emission of neutron-rich LCPs into the midrapidity region. These results are in agreement with previous works showing an increased production of neutron-rich fragments in the midrapidity region [17–26].

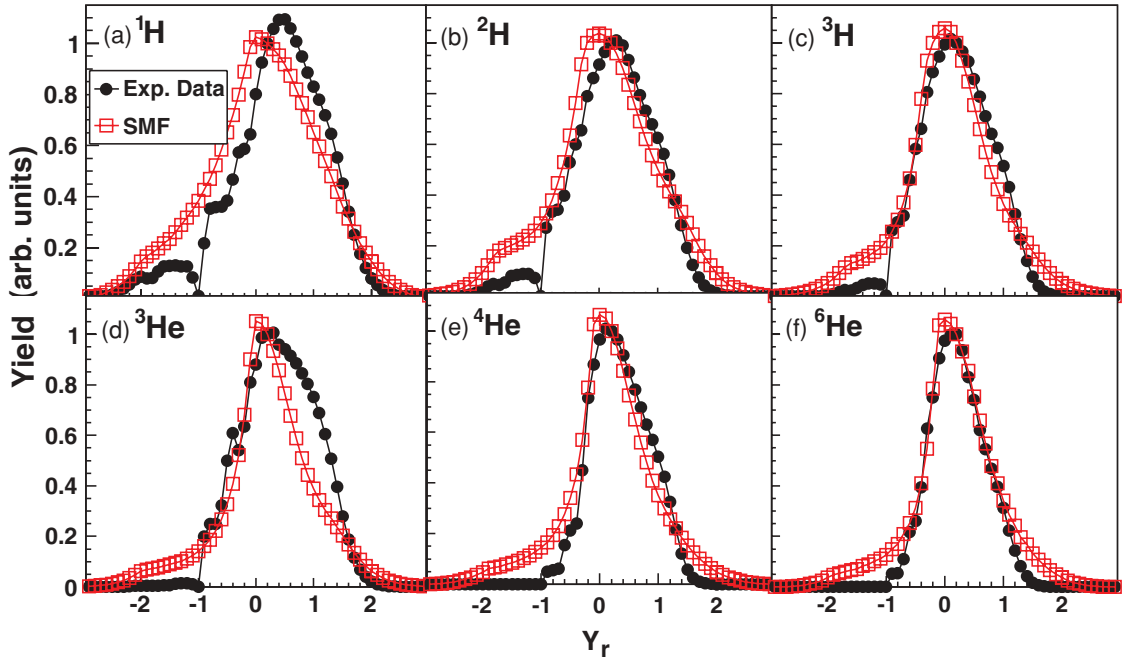

FIG. 1. (Color online) Reduced rapidity (Y_r) distribution for (a) ^{1}H, (b) ^{2}H, (c) ^{3}H, (d) ^{3}He, (e) ^{4}He, and (f) ^{6}He fragments from the 35 MeV/nucleon ^{64}Ni + ^{64}Ni reaction. The experimental data are shown as the solid black circles and the stiff-SMF calculation is shown as the open red squares. The detector thresholds have been applied to the SMF simulation. Each distribution has been normalized such that the yield at $Y_r = 0.0$ equals unity.

In comparing the $R_{\rm yield}^{\rm mid}$ results between systems relatively small differences are observed. Particularly, for the $Z = 1$ isotopes there is not a large difference in the midrapidity yield between the different reaction systems, as shown in Fig. 2. The most significant system effects are observed for the ^{6}He fragments where a large difference in the midrapidity yield is observed for the ^{64}Zn + ^{64}Zn system in comparison to the ^{64}Ni + ^{64}Ni and ^{70}Zn + ^{70}Zn systems. The relative midrapidity ^{6}He yield is suppressed in the least neutron-rich, ^{64}Zn, system, while the more neutron-rich systems show a strong enhancement of the midrapidity ^{6}He emission.

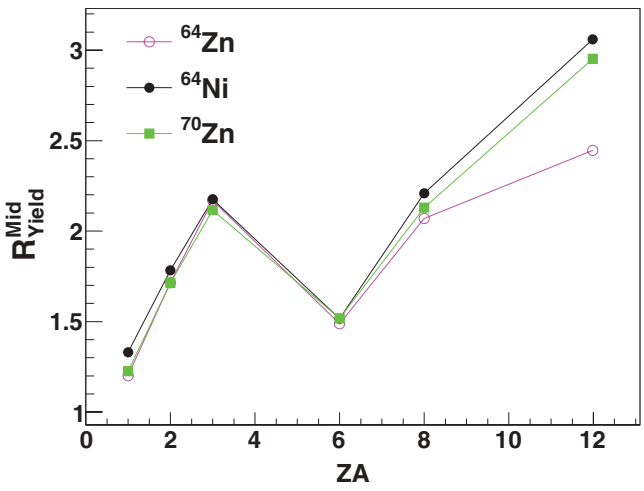

FIG. 2. (Color online) $R_{\rm yield}^{\rm mid}$ values are shown as a function of the charge times mass (ZA) for ^{1}H ($ZA = 1$), ^{2}H ($ZA = 2$), ^{3}H ($ZA = 3$), ^{3}He ($ZA = 6$), ^{4}He ($ZA = 8$), and ^{6}He ($ZA = 12$) particles.

The rapidity distributions for the LCPs calculated by the SMF model are compared to the experimental distributions in Fig. 1. The experimental detector thresholds have been applied to the SMF model calculation. The comparison shows that the SMF model is able to reasonably reproduce the experimental rapidity distributions. Both the simulation and the experiment demonstrate a strong preference for particle emission around the midrapidity region ($Y_r = 0.0$). The largest discrepancies are observed for the proton and the ^{3}He particles where the experimental distribution tends to have an increased forward rapidity yield relative to the SMF model. This difference could be attributed to the statistical decay of the QP at later stages of the reaction, which is not present in the SMF model, and has been shown to produce a significant fraction of the proton and ^{3}He yield [18,19].

The preferential emission of neutron-rich LCPs into the midrapidity region can be examined with the SMF model by examining the $R_{\rm yield}^{\rm mid}$ values, as shown in Fig. 3. In comparison to the experimental data, the SMF calculation, in general, overestimates the midrapidity enhancement of the LCPs. As mentioned, this may be attributable to the lack of QP decay, which would lower the $R_{\rm yield}^{\rm mid}$ values. However, the SMF calculations do show an increasing midrapidity yield for the more neutron-rich LCPs. In examining the isotopic trends, the SMF model shows a very similar trend for the $Z = 1$ isotopes as the experimental data. A strong increase in the ^{3}H midrapidity yield is observed relative to the proton yield. For the $Z = 2$ isotopes, the SMF model shows an increased $R_{\rm yield}^{\rm mid}$ with increasing neutron content of the fragments; however,

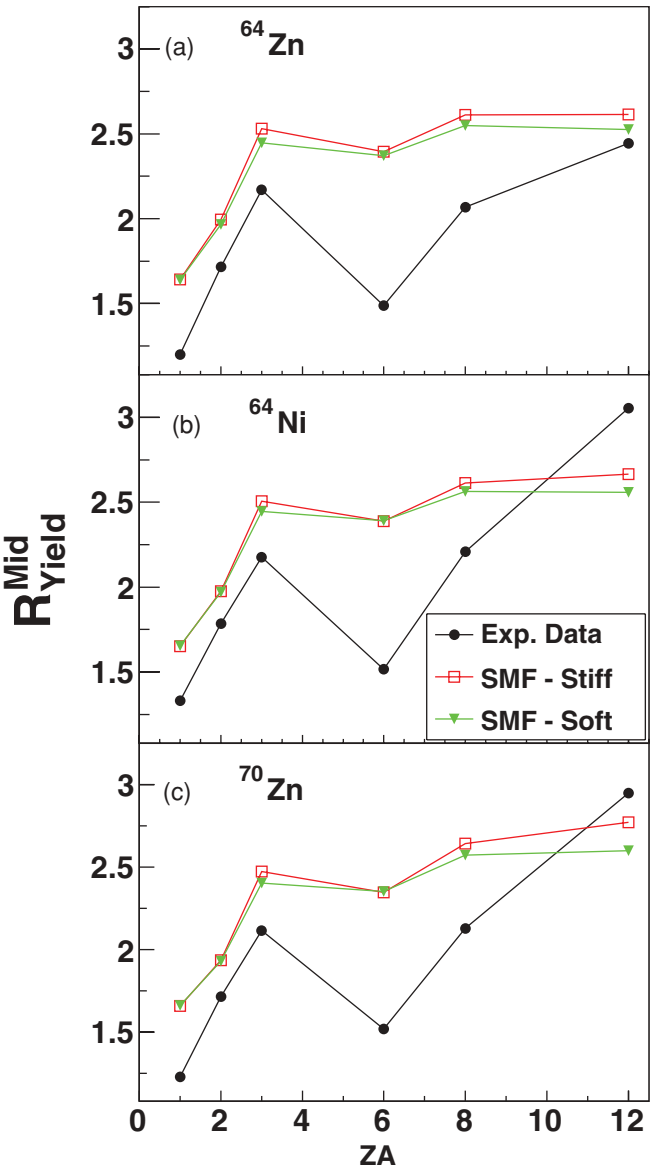

FIG. 3. (Color online) Comparison of the $R_{\text{yield}}^{\text{mid}}$ values from the experimental data (solid black circles) with the stiff (open red squares) and soft (solid green triangles) SMF calculation. The results from the three reaction systems are shown [panels (a)–(c)] and are plotted as a function of the charge times mass (ZA) of the LCPs.

the magnitude of the increase is smaller than that observed in the experimental data. Similarly, the isobaric comparison from the SMF calculation shows the same trend as the experimental data, with an increased midrapidity yield of the neutron-rich ^{3}H fragments relative to the ^{3}He fragments, yet the magnitude of the difference is much smaller than that observed in the experiment. Even though there are clear differences between the theory and the experiment, the results demonstrate the ability of the SMF model to correctly predict the enhanced particle production (Fig. 1) and neutron enrichment (Fig. 3) of the midrapidity region. Also, the impact of the density dependence of the symmetry energy can be seen in Fig. 3, where an increased midrapidity yield for the neutron-rich ^{3}H and ^{6}He isotopes is observed with a stiff density dependence of the symmetry energy.

B. Transverse flow

The transverse flow is often quantified as the slope of the average in-plane momentum, $\langle P_x \rangle$, over the midrapidity region. In Fig. 4, the average in-plane momentum per nucleon is plotted as a function of the reduced rapidity (Y_r), for the different isotopically identified LCPs. The solid line shown in each panel represents a linear fit over the region $-0.35 \leqslant Y_r \leqslant 0.35$. The extracted slope of the linear fit represents the transverse flow of the LCPs and is referred to as the flow parameter. This range was chosen because the smooth curvature of the $\langle P_x/A \rangle$ changes near $Y_r = -0.35$ owing to the backward angle detector thresholds. The error in the flow parameter was calculated from the error in the linear fit. Systematic errors associated with the fit range were estimated to be at most $+1$ and -0.4 (MeV/c)/A, by varying the fit range between $-0.4 \leqslant Y_r \leqslant 0.4$ and $-0.15 \leqslant Y_r \leqslant 0.15$. Systematic error from the SMF model was negligible at $+0.3$ and -0.2 (MeV/c)/A. Unless noted, only the fit error is presented in the results below.

The transverse flow of the $Z = 1$ and $Z = 2$ particles is presented first to examine the dependence of the flow on the mass, charge, and isospin content of the system. Additionally, this provides an opportunity to compare our results with those of Pak *et al.* [38] in a relatively straightforward manner. In Fig. 5 the $Z = 1$ and $Z = 2$ transverse flow is shown as a function of the neutron-to-proton ratio of the colliding system, $(N/Z)_{\text{sys}}$. Focusing on the ^{64}Ni + ^{64}Ni ($N/Z = 1.28$) and ^{64}Zn + ^{64}Zn ($N/Z = 1.13$) systems, a clear dependence on the $(N/Z)_{\text{sys}}$ is present. The results show an increased flow in the more neutron-rich system for the $Z = 1$ and $Z = 2$ particles. This is consistent with the previous observation by Pak *et al.* for $Z = 1$–3 fragments from systems with the same mass (A_{sys}) [38]. This observation was attributed to the isospin dependence of the mean-field and the nucleon-nucleon (nn) cross-sections [38]. However, based on a recent theoretical work, the observed difference may also be attributed to the increased Coulomb repulsion in the less neutron-rich system [68].

The results from the most neutron-rich ^{70}Zn ($N/Z = 1.33$) system show a decreased flow in comparison to the ^{64}Ni ($N/Z = 1.28$) system. The difference between the $A_{\text{sys}} = 128$ and $A_{\text{sys}} = 140$ systems can be qualitatively understood through the dependence of the transverse flow on the attractive mean-field, repulsive nn collisions and Coulomb repulsion. The flow should decrease as a function of A_{sys} [69], owing to the increased number of nn collisions (which scale with A_{sys}) relative to the attractive mean field (which scales with $A_{\text{sys}}^{2/3}$). Additionally, the flow from the ^{70}Zn system should be reduced owing to the increased Coulomb force in comparison to the ^{64}Ni system [68].

Last, the ^{64}Zn system and the ^{70}Zn system, which have the same Coulomb repulsion, have nearly equal flow. The mass dependence, mentioned above, would imply that the ^{70}Zn system should have a decreased flow. However, the observation

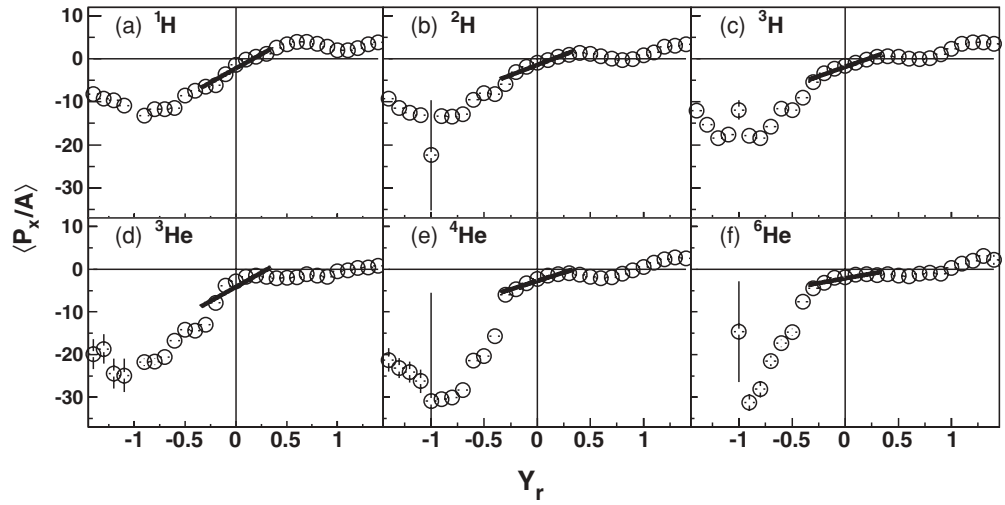

FIG. 4. Average in-plane momentum, $\langle P_x/A \rangle$, as a function of the reduced rapidity for (a) ^{1}H, (b) ^{2}H, (c) ^{3}H, (d) ^{3}He, (e) ^{4}He, and (f) ^{6}He particles. The results shown are from the midperipheral collisions of the ^{64}Ni + ^{64}Ni system. The solid black line represents a linear fit from $-0.35 \leqslant Y_r \leqslant 0.35$.

that the ^{70}Zn flow is not decreased demonstrates the effect of the isospin-dependent mean-field and *nn*-collision cross section [38]. The results from Fig. 5 exhibit the effects of the mass-, charge-, and isospin-dependent components of the transverse flow.

The results of Fig. 5 can be expanded upon through examining the flow per nucleon of isotopically identified LCPs, as shown in Fig. 6(a). Again, an enhancement in the transverse flow for the ^{64}Ni system is observed in comparison to the ^{64}Zn system demonstrating that the $(N/Z)_{\rm sys}$ dependence is also present for the $Z = 1$ (H) and $Z = 2$ (He) isotopes. Additionally, the results from the ^{70}Zn system show, for all isotopes except ^{3}H and ^{3}He, a decreased flow in comparison to the $A_{\rm sys} = 128$ systems, as expected from the $Z = 1$ and $Z = 2$ flow. It is interesting to note that the observed trend in the flow from the reaction systems, with ^{64}Ni flow > ^{64}Zn flow > ^{70}Zn flow, is not present for the ^{3}H and ^{3}He fragments where the flow from the ^{70}Zn system is larger than that from the ^{64}Zn system.

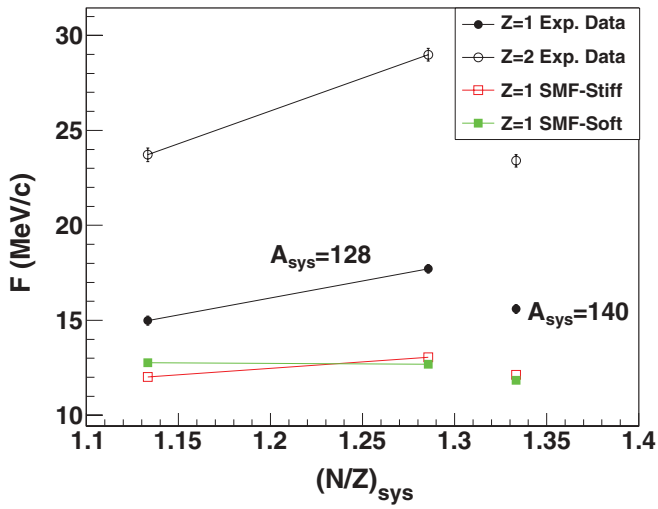

FIG. 5. (Color online) The experimental flow parameters (F) for the $Z = 1$ and $Z = 2$ fragments are shown as a function of the N/Z of the colliding system, $(N/Z)_{\rm sys}$, for the midperipheral collisions. The SMF model results are shown for the $Z = 1$ fragments for a stiff and soft $E_{\rm sym}(\rho)$. The ^{64}Zn and ^{64}Ni systems, $A_{\rm sys} = 128$, are connected by a solid line.

Isotopic and isobaric trends can also be explored from the extracted flow parameters in Fig. 6(a). A clear isotopic trend is observed in which the transverse flow per nucleon is decreasing as a function of the mass, or N/Z, of the isotope. For the $Z = 1$ isotopes, the protons exhibit the largest flow, followed by ^{2}H and then ^{3}H. Similarly, for the $Z = 2$ isotopes, the ^{3}He fragments have the largest flow followed by ^{4}He and then ^{6}He. Thus, the flow is seen to decrease as the neutron content of the isotopes increases. Examination of the transverse flow of the ^{3}H and ^{3}He fragments provides an isobaric comparison. The results, as shown in Fig. 6(a), demonstrate an enhancement in the ^{3}He flow in comparison to the ^{3}H flow. This, again, demonstrates a decreasing flow with increasing neutron content. Therefore, in comparing fragments with a constant charge (isotopes) or a constant mass (isobars), a consistent trend is observed showing a decreased flow for the more *n*-rich fragments. This suggests a differential movement of neutrons and protons in the dynamics of the midperipheral HICs below the balance energy.

The transverse flow extracted from the SMF model calculations was compared to the experimental results. Even though the simulation was stopped at 120 fm/c, previous theoretical results have shown that the magnitude of the transverse flow should saturate before 100 fm/c [70–73]. Also, because the beam energy is below the balance energy for the reaction systems the transverse flow extracted from the SMF model is negative. Therefore, to compare the SMF model to the experimental data, in which the flow is positive by convention [61], the sign of the flow from the SMF model was changed to be positive.

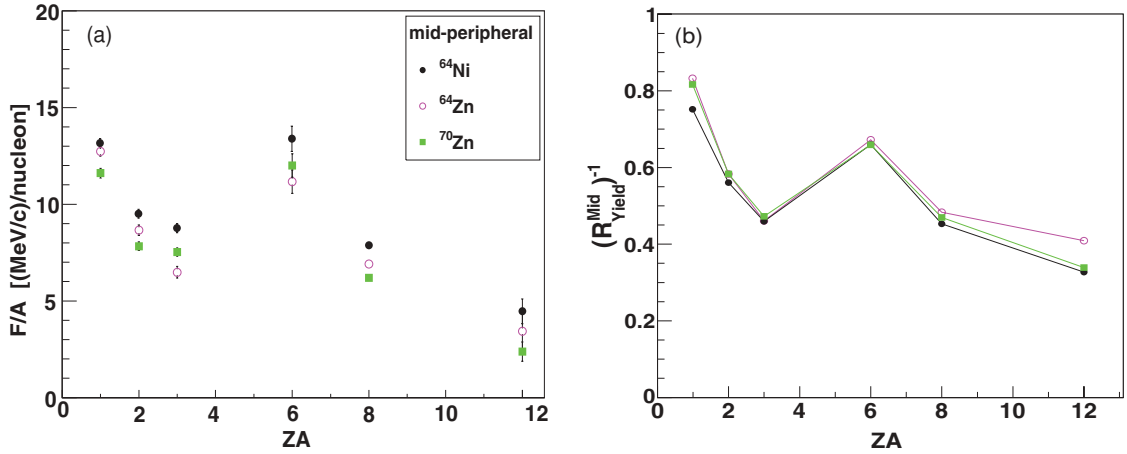

FIG. 6. (Color online) The extracted flow parameters (F) per nucleon (panel a) and inverse $R_{\rm yield}^{\rm mid}$ values (panel b) for the ^{1}H, ^{2}H, ^{3}H, ^{3}He, ^{4}He, and ^{6}He particles are shown as a function of the charge times mass (ZA) of the particle. Results are presented from ^{64}Ni, ^{64}Zn, and ^{70}Zn systems for midperipheral collisions as shown by the legend.

The $(N/Z)_{\rm sys}$ dependence of the $Z = 1$ flow from the SMF model is compared to the experimental data in Fig. 5. The magnitude of the $Z = 1$ flow is underestimated by the SMF model. However, the trend showing an increased flow for the ^{64}Ni system relative to the ^{64}Zn system is reproduced with the stiff-symmetry potential. This is not the case for the soft $E_{\rm sym}(\rho)$ calculation. This suggests a sensitivity to the low-density region of the symmetry potential, where the soft potential is more repulsive causing the more neutron-rich ^{64}Ni system to have a decreased flow relative to the ^{64}Zn system. It should be noted that other theoretical calculations have shown that, while the difference between the flow of equivalent mass system is sensitive to the symmetry energy, the dominant force is the Coulomb repulsion [68]. The $Z = 2$ results from the SMF model are not shown in Fig. 5 because there was no statistical difference in the flow between the three systems.

In Fig. 7 the LCP flow from the SMF model is compared to the experimental results. In general, the magnitude of the fragment flows from the SMF model are larger than that from the experiment. This may be attributable to the reaction-plane dispersion [62,74,75] present in the experimental analysis. However, the SMF model is able to reproduce the fragment flow trends reasonably well. Except for the proton flow, the isotopic trends show a decreasing flow with an increasing neutron content, as was observed in the experimental data. The SMF model is also able to reproduce the decreased difference in the ^{2}H and ^{3}H flow observed in the the ^{70}Zn experimental data [Fig. 7(c)]. The agreement between the fragment flow trends suggests that the SMF model correctly calculates a differential movement of the neutrons and protons in the mean field. Thus, in both the experiment and the theory a decreased flow is observed with increasing neutron content of the fragments.

The largest discrepancy between the experimental and SMF results is that the proton flow in the SMF model is decreased relative to the ^{2}H and ^{3}H flows. This may be attributed to the overproduction of the free nucleons owing to the lack of n-body correlations in the mean-field approach. Therefore, the additional free protons, which in reality should have been correlated with other nucleons, will decrease the flow relative to the correlated nucleons which are identified as fragments through the coalescence procedure.

The SMF model provides the opportunity to examine the sensitivity of the fragment flows to the density dependence of the symmetry energy. In Fig. 7 the results from the SMF model are shown with both a stiff and a soft $E_{\rm sym}(\rho)$. In general, the flow is decreased in the soft case, which can be attributed to the low-density behavior of the symmetry potential. As discussed above, at low density the soft-symmetry potential is more repulsive for neutrons and will, therefore, decrease the flow.

The difference between the ^{3}H and the ^{3}He flow also appears to be sensitive to $E_{\rm sym}(\rho)$, as predicted previously by Scalone *et al.* [42]. In Fig. 7 the stiff-symmetry potential produces a larger ^{3}He flow than ^{3}H flow, while the opposite is shown with the soft-symmetry potential for the ^{64}Ni and ^{70}Zn systems. In the ^{64}Zn system, the ^{3}H-^{3}He difference is not very sensitive to $E_{\rm sym}(\rho)$ because the asymmetry of the system is lower and therefore the magnitude of the symmetry potential is smaller. It is also interesting to note that the ^{3}H-^{3}He differences appear to be more sensitive to the density dependence of the symmetry energy than the free neutron-proton flows.

To quantitatively compare the ^{3}H-^{3}He flow between the experiment and SMF calculations the relative difference was calculated as

$$R_{^{3}\mathrm{He}\text{-}^{3}\mathrm{H}} = \frac{F^{^{3}\mathrm{He}} - F^{^{3}\mathrm{H}}}{F^{^{3}\mathrm{He}} + F^{^{3}\mathrm{H}}}, \tag{3}$$

where $F^{^{3}\mathrm{He}}$ and $F^{^{3}\mathrm{H}}$ represent the flow parameter extracted for the ^{3}He and ^{3}H fragments. Thus, if $R_{^{3}\mathrm{He}\text{-}^{3}\mathrm{H}}$ is greater (less) than 0 than the ^{3}He flow is larger (smaller) than the ^{3}H flow. In Fig. 8, $R_{^{3}\mathrm{He}\text{-}^{3}\mathrm{H}}$ is shown from the experiment (blue fill area) and SMF model (circles) for the midperipheral collisions. The width of the blue fill area represents the fit error in extracting the transverse flow. The estimated systematic

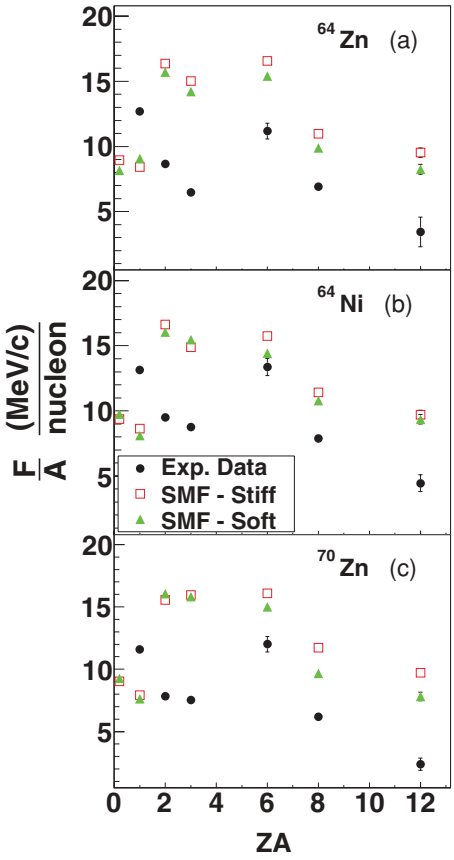

FIG. 7. (Color online) Flow parameter (F) per nucleon is shown as a function of the charge times mass (ZA) for the midperipheral collisions. The experimental data (black circles) is shown in comparison to the SMF model results, for both a stiff (red squares) and soft (green triangles) parametrization of the symmetry energy. The free neutron flow from the SMF model is offset with a $ZA = 0.1$ for clarity.

error in the experimental flow was accounted for and is shown by the dashed line. The largest uncertainty comes from the statistical/systematic error present in the ^{3}He flow. The SMF model results are shown both with (black circles) and without (gray circles) applying the detector thresholds. The results from the stiff- and soft-symmetry energy parametrizations are shown for each system as the closed and open circles, respectively.

The SMF model results, with and without the detector thresholds, demonstrate a sensitivity of the ^{3}H-^{3}He flow to the density dependence of the symmetry energy, specifically for the more neutron-rich ^{64}Ni and ^{70}Zn systems. Applying the detector thresholds to the simulated data produced an overall enhancement in the magnitude of $R_{^3\mathrm{He}\text{-}^3\mathrm{H}}$, moving it in closer agreement with the experiment. In general, the ^{3}H-^{3}He difference is underestimated by the SMF model. However, a stiff density dependence of the symmetry energy provides the better agreement with the experimental data in all cases. While the SMF calculations do not reproduce the experimental data on absolute scale, the large $R_{^3\mathrm{He}\text{-}^3\mathrm{H}}$ values from the experiment favor the stiff form of $E_{\mathrm{sym}}(\rho)$. Thus, the results indicate that the LCP flow is likely a sensitive observable to the nuclear EoS.

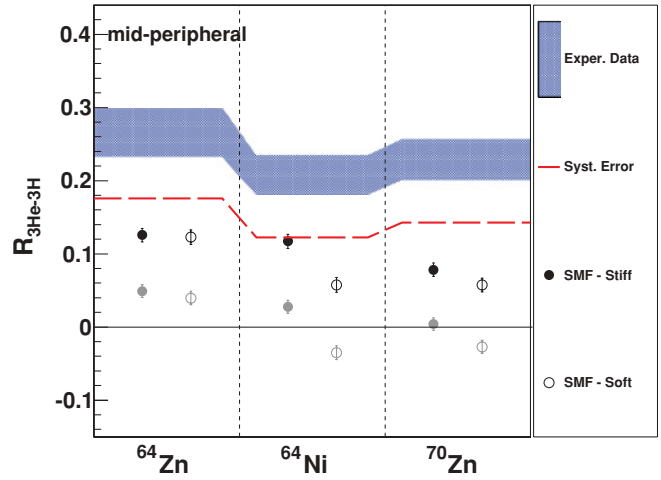

FIG. 8. (Color online) $R_{^3\mathrm{He}\text{-}^3\mathrm{H}}$, from Eq. (3), is calculated from the ^{64}Ni, ^{64}Zn, and ^{70}Zn systems for the midperipheral collisions. The results from the experimental data, including the fit error, are represented by the faded blue (gray) region. The estimated systematic error in the experimental results is represented by the red dashed line. The SMF results are shown with (black circles) and without (gray circles) applying the detector thresholds. As described by the legend, results with a soft and stiff density dependence of the symmetry energy are shown from the SMF model.

C. Correlation between midrapidity yield and transverse flow

The midrapidity yield and transverse flow should be connected because both are observables associated with the emission of particles in between the QP and QT. For comparison, the two observables are shown, side by side, in Fig. 6. A clear correlation is shown between the transverse flow [Fig. 6(a)] and the inverse of $R_{\mathrm{yield}}^{\mathrm{mid}}$ [Fig. 6(b)] of the LCPs. Nearly identical isotopic and isobaric trends are present. The results demonstrate that the increased relative midrapidity emission [a decrease in $(R_{\mathrm{yield}}^{\mathrm{mid}})^{-1}$] coincides with a decreased transverse flow. A possible explanation for the correlation based on the *isospin migration* phenomenon [28,30] is presented below in context of the SMF model results.

The ^{3}H-^{3}He flow results discussed above can be interpreted in terms of a more neutron-rich emission from the neck region in the stiff case [28]. The lower value of the stiff-symmetry potential, with respect to the soft, during the expansion phase of the system leads to less repulsive dynamics, associated with a generally larger flow of the LCPs (see Fig. 7). At the same time, the neutron excess is transferred toward the low-density neck region, from which LCPs eventually emerge. The latter mechanism (isospin migration), which is sensitive to the derivative of the symmetry energy just below normal density, is more effective in the stiff case [28] producing a more neutron-rich neck region. This is confirmed by examining the $R_{\mathrm{yield}}^{\mathrm{mid}}$ values of the LCPs calculated from both the stiff- and the soft-symmetry potential, as shown in Fig. 3. An increase in the midrapidity yield of the neutron-rich fragments, ^{3}H and ^{6}He, is observed in the stiff case, relative to the soft. The larger asymmetry of the neck region in the stiff case also explains the larger repulsion seen for ^{3}H, with respect to ^{3}He, thus producing a decreased flow (see Figs. 7 and 8). This suggests

a clear connection between the isobaric trends observed in the LCP flow and $R_{\rm yield}^{\rm mid}$ results.

The importance of the neck dynamics, suggested by the SMF model, can also provide insight into the observation of the decreased flow with increasing neutron content of the LCPs (see Figs. 6 and 7). The isospin migration phenomenon represents the movement of neutrons and protons in opposite directions owing to a density gradient. Thus, neutrons preferentially move toward the low-density neck region, while protons will travel toward a higher-density region (near the saturation density), such as the QP. If the transverse flow is thought to represent the movement, or flow, of particles following the QP and the QT, then the proton movement, owing to the isospin migration, may enhance the transverse flow. Likewise, the opposite movement of neutrons could diminish the flow. Thus, upon coalescence of the free nucleons the proton-rich fragments, such as ^{1}H and ^{3}He, would exhibit a larger flow with respect to neutron-rich fragments, such as ^{3}H and ^{6}He. Therefore, the occurrence of isospin migration can account for the strong correlation observed between the LCP flow [Fig. 6(a)] and midrapidity emission [Fig. 6(b)]. Further investigation of this concept is required, such as examining these observables in isospin asymmetric systems where *isospin diffusion* [76] is present and may enhance the observed trends.

IV. CONCLUSIONS

In summary, the midrapidity emission and transverse flow of LCPs from 35 MeV/nucleon Zn and Ni systems have been studied. Examination of the rapidity distributions of the LCPs demonstrated a strong preference for emission around the midrapidity region. Further examination showed an enhanced emission of the more neutron-rich isotopes and isobars in the midrapidity region, relative to the QP region, in comparison to the less neutron-rich LCPs. The transverse flow of the LCPs was also extracted and strong isotopic and isobaric trends, in which the flow decreased with increasing neutron content of the fragments. A strong correlation between the enhancement of the relative yield of the neutron-rich fragments in the midrapidity region and the decreased flow of the neutron-rich fragments was shown.

The SMF model was used to examine the midrapidity emission and transverse flow results, as well as the sensitivity of these observables to the density dependence of the symmetry energy. Many of the experimental trends were well reproduced by the SMF model, though, significant differences exist on absolute scale. The present studies demonstrate that both the midrapidity yield and transverse flow showed sensitivity to the density dependence of the symmetry energy. Additionally, the SMF results indicated that the correlation between the relative midrapidity yield and flow of the LCPs could be attributed to the occurrence of isospin migration.

ACKNOWLEDGMENTS

We thank the staff members of the Texas A&M Cyclotron Institute for the excellent beam quality. This work was supported in part by the Robert A. Welch Foundation through Grant No. A-1266 and the Department of Energy through Grant No. DE-FG03-93ER40773. We also thank the Target Lab at Argonne National Laboratory for the fabrication of the ^{70}Zn target and the Laboratory for Molecular Simulation at Texas A&M University for providing computer time for the SMF calculations.

[1] S. Shlomo, V. M. Kolomietz, and G. Colo, Eur. Phys. J. A **30**, 23 (2006).
[2] C. Fuchs and H. H. Wolter, Eur. Phys. J. A. **30**, 5 (2006).
[3] B. A. Li, L. W. Chen, and C. M. Ko, Phys. Rep. **464**, 113 (2008).
[4] M. B. Tsang, Y. Zhang, P. Danielewicz, M. Famiano, Z. Li, W. G. Lynch, and A. W. Steiner, Phys. Rev. Lett. **102**, 122701 (2009).
[5] D. V. Shetty, S. J. Yennello, and G. A. Souliotis, Phys. Rev. C **76**, 024606 (2007).
[6] S. Kowalski *et al.*, Phys. Rev. C **75**, 014601 (2007).
[7] J. M. Lattimer and M. Prakash, Science **304**, 536 (2004).
[8] B. A. Li, Nucl. Phys. A **708**, 365 (2002).
[9] T. Klahn *et al.*, Phys. Rev. C **74**, 035802 (2006).
[10] R. J. Furnstahl, Nucl. Phys. A **706**, 85 (2002).
[11] J. R. Stone, J. C. Miller, R. Koncewicz, P. D. Stevenson, and M. R. Strayer, Phys. Rev. C **68**, 034324 (2003).
[12] B. A. Li, Phys. Rev. Lett. **88**, 192701 (2002).
[13] A. W. Steiner, M. Prakash, J. M. Lattimer, and P. J. Ellis, Phys. Rep. **411**, 325 (2005).
[14] C. P. Montoya *et al.*, Phys. Rev. Lett. **73**, 3070 (1994).
[15] R. Wada *et al.*, Nucl. Phys. A **548**, 471 (1992).
[16] J. Toke *et al.*, Nucl. Phys. A **583**, 519 (1995).
[17] M. Di Toro, A. Olmi, and R. Roy, Eur. Phys. J. A **30**, 65 (2006).
[18] J. Lukasik *et al.*, Phys. Rev. C **55**, 1906 (1997).
[19] E. Plagnol *et al.*, Phys. Rev. C **61**, 014606 (1999).
[20] D. Theriault *et al.*, Phys. Rev. C. **74**, 051602(R) (2006).
[21] J. F. Dempsey *et al.*, Phys. Rev. C **54**, 1710 (1996).
[22] S. Piantelli *et al.*, Phys. Rev. C **76**, 061601(R) (2007).
[23] R. Planeta *et al.*, Phys. Rev. C. **77**, 014610 (2008).
[24] S. Hudan *et al.*, Phys. Rev. C **71**, 054604 (2005).
[25] R. Laforest, E. Ramakrishnan, D. J. Rowland, A. Ruangma, E. M. Winchester, E. Martin, and S. J. Yennello, Phys. Rev. C **59**, 2567 (1999).
[26] D. V. Shetty *et al.*, Phys. Rev. C **68**, 054605 (2003).
[27] J. Rizzo, M. Colonna, V. Baran, M. Di Toro, H. H. Wolter, and M. Zielinska-Pfabe, Nucl. Phys. A **806**, 79 (2008).
[28] R. Lionti, V. Baran, M. Colonna, and M. Di Toro, Phys. Lett. B **625**, 33 (2005).
[29] V. Baran, M. Colonna, M. Di Toro, V. Greco, M. Zielinska-Pfabe, and H. H. Wolter, Nucl. Phys. A **703**, 603 (2002).
[30] V. Baran, M. Colonna, and M. Di Toro, Nucl. Phys. A **730**, 329 (2004).
[31] L. G. Sobotka, Phys. Rev. C **50**, 1272(R) (1994).
[32] P. Danielewicz, R. Lacey, and W. G. Lynch, Science **298**, 1592 (2002).
[33] D. J. Magestro, W. Bauer, and G. D. Westfall, Phys. Rev. C **62**, 041603(R) (2000).
[34] B. A. Li, C. M. Ko, and W. Bauer, Int. J. Mod. Phys. E **7**, 147 (1998).
[35] M. Di Toro, S. J. Yennello, and B. A. Li, Eur. Phys. J. A **30**, 153 (2006).

[36] V. Baran, M. Colonna, V. Greco, and M. Di Toro, Phys. Rep. **410**, 335 (2005).
[37] Z. Kohley *et al.*, Phys. Rev. C **82**, 064601 (2010).
[38] R. Pak *et al.*, Phys. Rev. Lett. **78**, 1022 (1997).
[39] R. Pak *et al.*, Phys. Rev. Lett. **78**, 1026 (1997).
[40] C. Liewen, Z. Fengshou, and J. Genming, Phys. Rev. C **58**, 2283 (1998).
[41] B. A. Li, Z. Ren, C. M. Ko, and S. J. Yennello, Phys. Rev. Lett. **76**, 4492 (1996).
[42] L. Scalone, M. Colonna, and M. Di Toro, Phys. Lett. B **461**, 9 (1999).
[43] B. A. Li, Phys. Rev. Lett. **85**, 4221 (2000).
[44] G. C. Yong, B. A. Li, and L. W. Chen, Phys. Rev. C **74**, 064617 (2006).
[45] B. A. Li, Nucl. Phys. A **708**, 365 (2002).
[46] W. Trautmann, M. Chartier, Y. Leifels, R. C. Lemmon, Q. Li, J. Lukasik, A. Pagano, P. Pawlowski, P. Russotto, and P. Wu, Prog. Part. Nucl. Phys. **62**, 425 (2009).
[47] W. Trautmann, M. Chartier, Y. Leifels, R. C. Lemmon, Q. Li, J. Lukasik, A. Pagano, P. Pawlowski, P. Russotto, and P. Z. Wu, arXiv:0907.2822v1 [nucl-ex].
[48] G. C. Yong, B. A. Li, L. W. Chen, and X. C. Zhang, Phys. Rev. C **80**, 044608 (2009).
[49] J. Rizzo, M. Colonna, M. Di Toro, and V. Greco, Nucl. Phys. A **732**, 202 (2004).
[50] V. Giordano, M. Colonna, M. Di Toro, V. Greco, and J. Rizzo, Phys. Rev. C **81**, 044611 (2010).
[51] S. Wuenschel *et al.*, Nucl. Instrum. Methods Phys. Res. A **604**, 578 (2009).
[52] R. P. Schmitt *et al.*, Nucl. Instrum. Methods Phys. Res. A **354**, 487 (1995).
[53] J. Pouthas *et al.*, Nucl. Instrum. Methods Phys. Res. A **357**, 418 (1995).
[54] K. Kwiatkowski *et al.*, Nucl. Instrum. Methods Phys. Res. A **360**, 571 (1995).
[55] S. Wuenschel, K. Hagel, L. W. May, R. Wada, and S. J. Yennello, AIP Conf. Proc. **1099**, 816 (2009).
[56] L. Tassan-Got, Nucl. Instrum. Methods Phys. Res. B **194**, 503 (2002).
[57] R. Wada *et al.*, Phys. Rev. C **69**, 044610 (2004).
[58] S. Wuenschel, Ph.D. thesis, Texas A&M University, 2009.
[59] G. D. Westfall, Nucl. Phys. A **630**, 27 (1998).
[60] M. Papa, G. Giuliani, and A. Bonasera, J. Comput. Phys. **208**, 403 (2005).
[61] W. K. Wilson, R. Lacey, C. A. Ogilvie, and G. D. Westfall, Phys. Rev. C **45**, 738 (1992).
[62] P. Danielewicz and G. Odyniec, Phys. Lett. B **157**, 146 (1985).
[63] D. Cussol *et al.*, Phys. Rev. C **65**, 044604 (2002).
[64] C. A. Ogilvie *et al.*, Phys. Rev. C **40**, 2592 (1989).
[65] P. Chomaz, M. Colonna, and J. Randrup, Phys. Rep. **389**, 263 (2004).
[66] E. Santini, T. Gaitanos, M. Colonna, and M. Di Toro, Nucl. Phys. A **756**, 468 (2005).
[67] A. Bonasera and L. P. Csernai, Phys. Rev. Lett. **59**, 630 (1987).
[68] S. Gautam and A. D. Sood, Phys. Rev. C **82**, 014604 (2010).
[69] G. D. Westfall *et al.*, Phys. Rev. Lett. **71**, 1986 (1993).
[70] A. Bonasera, F. Gulminelli, and J. Molitoris, Phys. Rep. **243**, 1 (1994).
[71] R. Nebauer and J. Aichelin, Nucl. Phys. A **650**, 65 (1999).
[72] A. D. Sood and R. K. Puri, Phys. Rev. C **69**, 054612 (2004).
[73] J. Zhang, S. Das Gupta, and C. Gale, Phys. Rev. C **50**, 1617 (1994).
[74] A. Andronic, J. Lukasik, W. Reisdorf, and W. Trautmann, Eur. Phys. J. A **30**, 31 (2006).
[75] J. Lukasik and W. Trautmann, arXiv:nucl-ex/0603028v1.
[76] M. B. Tsang *et al.*, Phys. Rev. Lett. **92**, 062701 (2004).